Operating Characteristics of a 60- and 10-cm Electric Arc-Driven Shock Tube—Part II: The Driven Section

Surendra P. Sharma* and Chul Park*
NASA Ames Research Center, Moffett Field, CA 94035

This is the second part of a two-part paper describing the operating characteristics of the electric arc-driven shock-tube facilities at NASA Ames Research Center. This part discusses the performance of the driven sections when the facility is used as a tool to produce a low-density nonequilibrium flow and when used as a shock tunnel. Specifically, the paper discusses the cleanliness of the driven flow at low densities, and the deviation from the equilibrium conditions at the test section of the shock-tunnel flow.

Nomenclature

a = speed of sound
A = cross-sectional area of nozzle, m^2
A^* = cross-sectional area of nozzle throat, m^2
C_p = specific heat at constant pressure
C_v = specific heat of trigger wire
h = flow enthalpy, J/kg
K_f = forward (dissociation or ionization) rate coefficient, cm^3 mole^{-1} s^{-1}
K_r = recombination rate coefficient, cm^6 mole^{-2} s^{-1}
P_1 = initial charging pressure in the driven tube
T = gas temperature, K
V_∞ = equivalent flight speed or test section flow speed, m/s
x = distance from throat along nozzle, m
( ) = species number density

Subscripts
1 = initial driven-tube condition
2 = behind the primary shock
4 = initial driver condition
5 = reflected shock
∞ = test section

I. Introduction

IN the accompanying Sec. I of this paper,[1] we have described the operating envelope and characteristics of the driver for the 60- and 10-cm electric arc-driven shock-tube facility at NASA Ames Research Center. In this part, Sec. II, we will discuss the usefulness of the facility in two fields of application: 1) in the production of the low-density nonequilibrium test flows, and 2) in the production of high Mach number flows by operating as a shock tunnel. In the production of the low-density nonequilibrium test flows, the most important phenomenon concerns metallic impurities in the test flows. The metallic impurity problem becomes the main roadblock at low densities because the relative magnitude of the impurity effects become larger at low densities. Therefore, the paper first focuses on the efforts made to eliminate metallic impurities in the test flows. In producing a hypersonic flow in the test section of a shock tunnel, the most important issue concerns the degree of nonequilibrium in the test flow: due to freezing in the nozzle, the test-section flow tends to be out of equilibrium. The paper describes how close the produced flow is to equilibrium. Using a characteristic time criterion for sudden freezing of chemical reactions in a nozzle, the paper shows that the flow in the test section is likely to be close to being in chemical and thermal equilibrium in the range of enthalpies corresponding to a flight speed of 5 km/s or less.

II. Production of Clean Flow in Driven Section

In order to study chemical kinetics at low densities, one usually resorts to spectroscopic techniques by which radiation emission, absorption, or scattering characteristics are studied. One prerequisite for doing so is that the test gas sample produced behind the primary shock is spectroscopically clean. For this reason, spectra have been taken in both shock tubes using 99.99% pure nitrogen as the test gas. The 0.01% impurity consisted mostly of oxygen, carbon dioxide, and hydrocarbons. In these runs, the tube was evacuated to 0.6 μm Hg, and was held at a leak rate of 0.04 μm Hg/min. In Fig. 1, the spectra obtained in the 60-cm tube using nitrogen as the test gas at $P_1 = 0.1$ Torr, at shock velocity of 12 km/s, are shown. The spectra looking through the sidewall were obtained using a 0.5-m focal length $f/1.5$ spectrograph designed by Borucki[2] which uses achromatic lenses. Because of the lenses, the shortest accessible wavelength was limited to about 3900 Å. The shutter was let open during the entire run, and so the spectra are a time integration of all emissions during the run, including those from the driver gas. The trigger wire in these runs were made of tungsten. The discharge is expected to vaporize the wire, and so one can expect to see the spectra of tungsten in the spectra obtained. Surprisingly, the spectra are devoid of tungsten, but contain radiation from iron (Fe), chromium (Cr), and sodium (Na). Molecular bands, such as the N_2^+ First Negative system below 4300 Å and the N_2 First Positive system above 5500 Å, are seen in the spectra, but are either of the same order in magnitude or weaker than those of the impurities. Gaseous impurities cannot be identified in the spectra presumably because their intensities are too weak.

The sodium radiation can be traced to the atmosphere. Schneider and Park[3] studied the sodium problem in detail, and concluded that the natural sodium chloride in the atmosphere, to a concentration of up to about 10^{11} cm^{-3}, can be adsorbed on the wall of the driven tube to produce one or more monolayers. During the pumping period, the sodium chloride desorbs. However, complete desorption is not likely unless the tube is heated. After the pumping is stopped and the test gas introduced, desorption still continues into the driven

Presented as Paper 88-0142 at the AIAA 26th Aerospace Sciences Meeting, Reno, NV, Jan. 11-14, 1988; received March 10, 1988; revision received Oct. 5, 1989.

*Research Scientist. Associate Fellow AIAA.

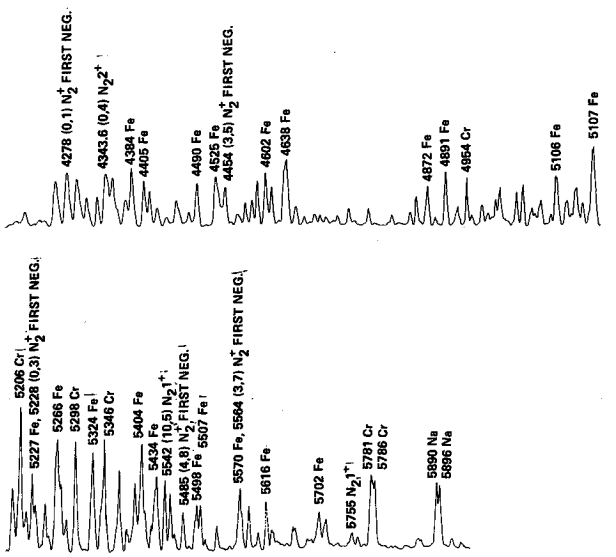

Fig. 1 The emission spectra of nitrogen produced in the 60-cm driven tube made of stainless steel, obtained by time integration.

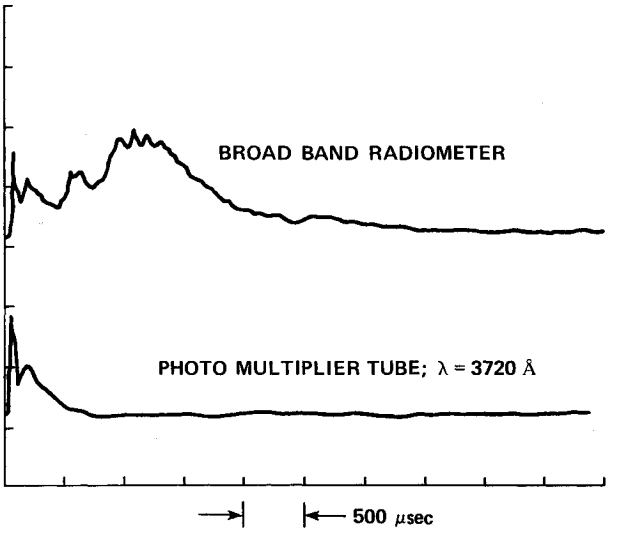

Fig. 2 Time record of radiation intensities taken in the 10-cm tube made of stainless steel. The broadband radiometer consisted of a silicon photoresistive detector of nearly flat repsonse over the wavelength range from 0.4–1 μm. The 3720 Å photomultiplier tube was integrating over a wavelength range of 40 Å. Initial driven-tube charging pressure = 0.1 Torr (nitrogen), shock velocity = 12.0 km/s, and the oscilloscope sweep rate = 500 μs/division.

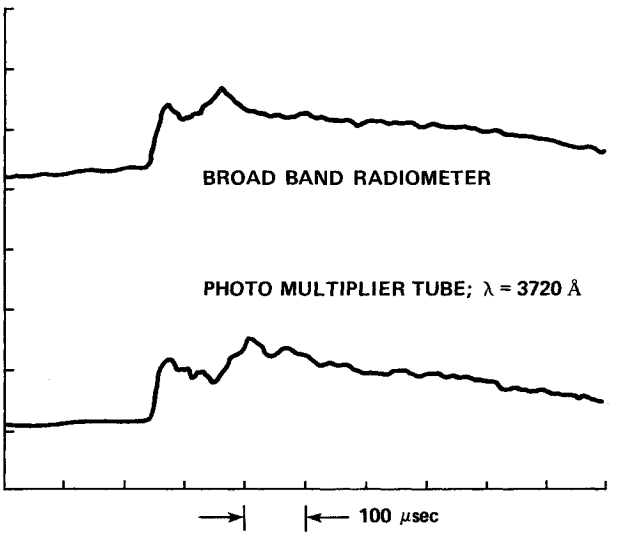

Fig. 3 Time record of radiation intensities taken in the 10-cm tube made of aluminum. The sensors are the same as in Fig. 2. Initial driven-tube charging pressure-0.1 Torr (nitrogen), shock velocity = 10.3 km/s, and the oscilloscope sweep rate = 500 μs/division.

gas. When the primary shock arrives, sodium chloride molecules dissociate to produce sodium atoms, which can radiate.

Little explanation can be offered for the origin of iron and chromium lines. In the experiment by Schneider and Park,[3] the metallic impurities were seen spectroscopically even though cold (without electric arc discharge) helium was used as the driver gas. Therefore, the metallic impurities originate at least partly from the driven gas or driven tube. One possible hypothesis is that iron and chromium in the stainless-steel driven tube dissolves in the thin layer of the organic acid coating the surface of the driven tube. The acid is produced by the mixing of the vacuum pump oil with atmospheric water, irradiated by the ultraviolet radiation of the test gas. Under such hypothesis, the only way to remove it was seen to be replacing the stainless-steel tube with another material. During the late 1950s and early 1960s, the researchers at AVCO[4] made their measurements of nonequilibrium radiation using electric arc-driven shock tubes whose driven tubes were made of aluminum. The spectra obtained in their tests show no discernible amount of radiation from such metallic impurities. To identify the source of the metallic impurities and to find a remedy, another driven tube was made out of aluminum alloy, and positioned in place of the stainless-steel driven tube. The tests were repeated with the aluminum driven tube with the 99.99% pure nitrogen as the test gas. No attempt was made to remove the gaseous impurities (oxygen, carbon dioxide, and hydrocarbons) from the test gas, because the problem of the possible gaseous impurities are presently not as serious as the problem of metallic impurities.

In order to monitor the amount of iron contamination, two monochromators were set at Fe lines at 3737 and 3720 Å. Bausch and Lomb 0.25-m focal length $f/5$ monochromators were used for this purpose. The entrance and exit slit widths were set such that the slit function was nearly a symmetrical triangle with an equivalent half-height width of 40.0 Å. A broad band (0.2–1.6 μm) radiometer was used to record the total radiation from the test gas. Figure 2 displays the signals from the radiometer and monochromator (3720 Å) recorded in the steel driven tube. The radiometer trace initially shows a peak indicating the arrival of the shock wave. The monochromator trace also shows a peak at the time of shock arrival. As the driver gas, following the shock, passes through the test section the radiometer signal rises again, indicating the arrival of the driver gas. However, the monochromator signal does not show any increase in the signal level, indicating that the peak in the monochromator signal at the time of shock arrival is essentially due to the presence of steel vapor in the test gas. It also indicates that the amount of steel vapors present in the driver gas is negligible.

Figure 3 displays the signals from the radiometer and monochromator set at 3720 Å obtained from the test with the aluminum driven tube. As is seen from the figure, the two signals follow an identical pattern, suggesting that the iron contamination, if there is any, is evenly distributed over the driver and driven gas. Since the same driver was used in both the experiments and we have established that the amount of iron contaminants in the driver gas is insignificant, it is concluded that the amount of Fe contaminant in the test gas produced in the aluminum tube is very small.

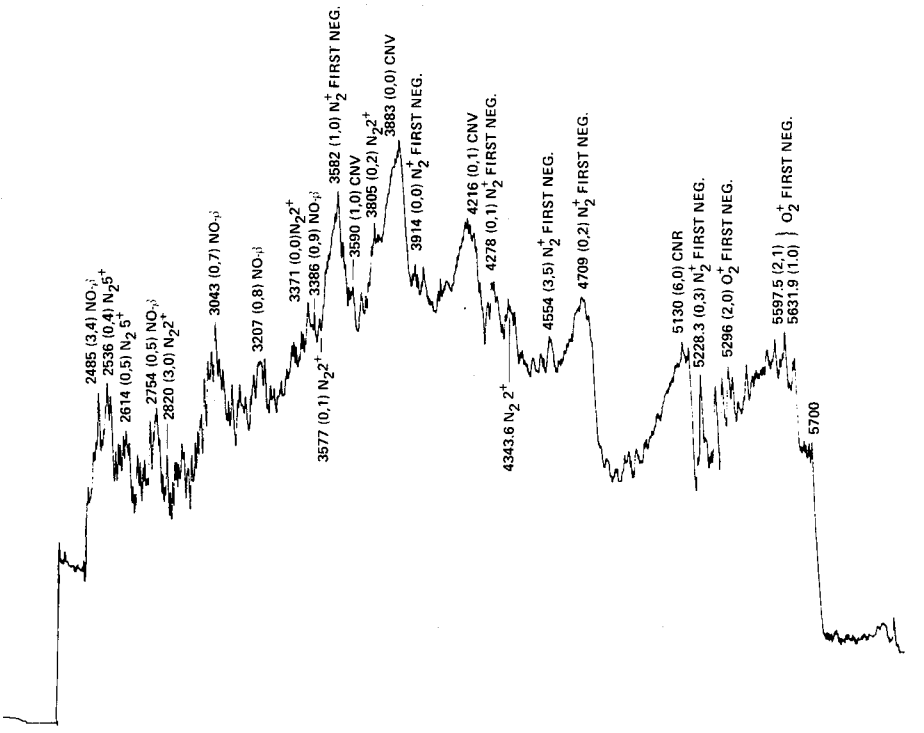

Fig. 4. The emission spectra produced in the 10-cm driven tube made of aluminum obtained by time integration. Initial driven-tube pressure = 0.1 Torr (nitrogen) and shock velocity = 10.3 km/s.

The spectra of test gas from the aluminum tube were recorded using a McPherson model 218 0.3-m focal length $f/5$ spectrometer with a 180 lines/mm grating. The system had a dispersion of 150 Å/mm with total recording width of 3750 Å, that is, from 2250–6000 Å. The slit width was 0.05 mm, corresponding to 7.5 Å resolution in the recorded spectra. Figure 4 displays the spectra of N_2 recorded at a shock velocity of 10.3 km/s at $P_1 = 0.1$ Torr. The spectra consist of vibrational bands from molecular species, CN, N_2, N_2^+, NO, and O_2^+. No iron or chromium lines are identifiable in the spectra. The peak at about 3883 Å is caused by the compounding of the (0,0) band of the CN violet system with band head at 3883 Å and the (0,0) band of the First Negative band of N_2^+ with band head at 3914.4 Å. The carbon element in the CN molecules is believed to have originated from the carbon dioxide and hydrocarbons contained in the test gas, vacuum pump oil vapors, and the mylar diaphragm. Near the red end of the spectra, the First Negative bands of O_2^+ with a band head at 5631.9 Å are seen. The oxygen molecules are believed to have originated mostly from the test gas. Presence of O_2 also explains the NO-β bands with band heads at 3207, 3043, and 2754 Å in the ultraviolet region. Overall, the spectrum is dominated by the molecular bands of N_2^+. Figures 3 and 4 show that the test gas produced in an aluminum driven tube does not contain metallic impurities to any significant amount. The present finding agrees with the results of the tests conducted at AVCO.[4]

A task remains presently to remove the hydrocarbon impurities from the test gas. Future tests are planned in which 1) the driven tube will be pumped using an oil-free turbomolecular pump, and 2) an aluminum diaphragm will be used in place of the mylar diaphragm. Instantaneous spectra will be taken using an intensified-gated (gating time ~5 ns), multichannel diode detector array. Total radiation (0.2–3 μm) using a custom-designed radiometer will also be measured.

III. Shock Tunnel Characteristics

The test-gas Mach number produced in a shock tube does not exceed 1.87 for a perfect gas and may approach 4 in a real gas, if dissociation and ionizations are present. Thus, the shock tubes, although simulating the thermodynamic and chemical processes occurring behind a shock wave in the hypersonic flight regime very well, do not simulate high Mach number flows. To simulate high Mach number flows, it is customary to let the shock-heated gas reach the end wall and develop a reflected shock wave and expand the gas in the reflected-shock region through a convergent-divergent nozzle. The enthalpy in the reflected-shock region is approximately twice that behind the primary shock in this range of high

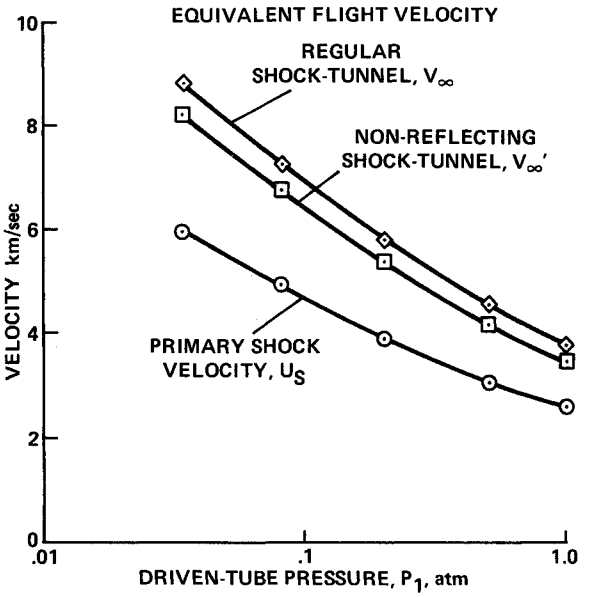

Fig. 5 Measured primary-shock velocities and calculated equivalent flight velocities of the produced flows corresponding to the measured primary-shock velocities in the regular and nonreflecting shock-tunnel modes, as functions of the initial driven-tube charging pressure P_1, at a fixed capacitor setting of 20 kV and 172 kJ.

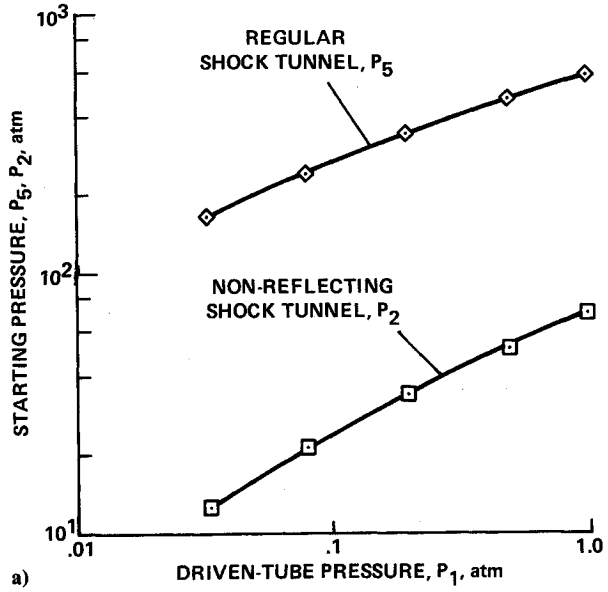

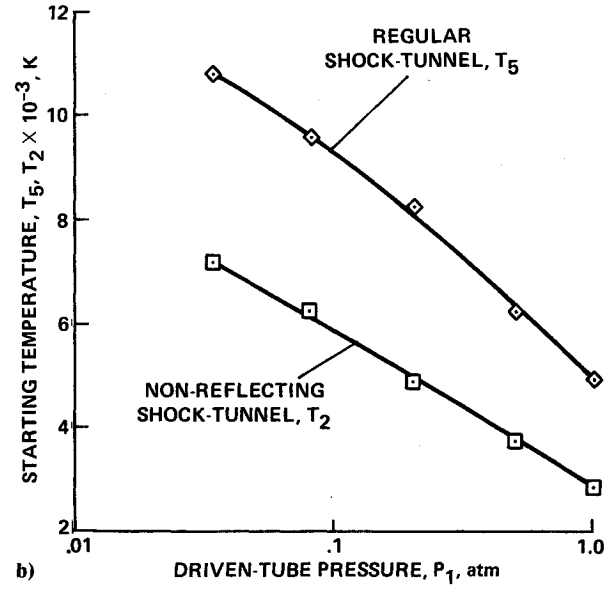

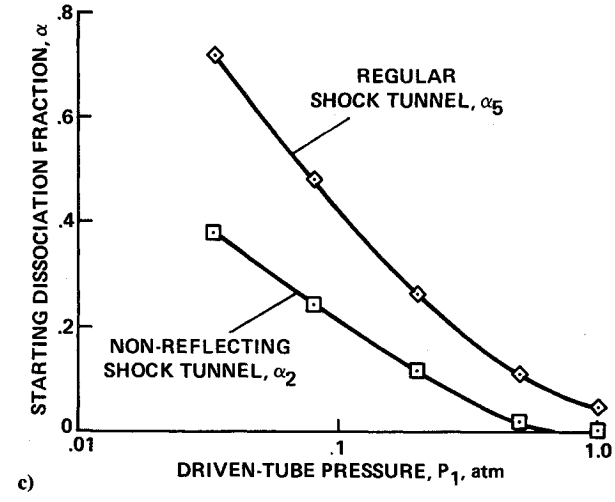

Fig. 6 Calculated starting (entrance to the expanding nozzle) conditions of the regular and nonreflecting shock-tunnel modes corresponding to the measured shock velocities, as functions of the initial driven-tube charging pressure P_1, at a fixed capacitor setting of 20 kV and 172 kJ: a) pressure; b) temperature; and c) dissociation fraction.

shock Mach numbers. Such a facility is known as the (regular) shock tunnel. Alternatively, the end wall can be removed, and the flow behind the primary shock can be expanded directly through a hypersonic nozzle. Such a facility is known as the nonreflecting shock tunnel. Unlike the regular shock tunnel, the static enthalpy of the flow at the starting point of the expansion in a nonreflecting shock tunnel is only that behind the primary shock. However, the kinetic energy is considerable: it is over 80% of the static enthalpy. Thus, the total enthalpy of the flow in the nonreflecting shock tunnel is over 80% of that in the regular shock tunnel.

Since the speed of the primary shock wave is approximately proportional to a_4, the speed of sound of the driver gas, and since the enthalpies of the shock tunnels are proportional to that behind the primary shock, the enthalpies of the shock-tunnel flows are dictated also by a_4. As mentioned in Sec. I of this paper, the electric arc driver produces the highest attainable a_4. Hence, the enthalpy produced is also the highest with an arc driver.

The 10-cm tube of the facility is equipped with a regular shock-tunnel nozzle of area ratio 1000, which is conical in shape and is 1.8 m in length. The nozzle had been used for the purpose of developing a gasdynamic laser.[5] Another smaller nozzle of area ratio 10 has been used for the study of radiation in the flow around the Galileo Probe.[6] The large nozzle has never been used for the purpose of testing models in the test section. As mentioned in Sec. I, performance of the shock tunnels is of interest for future applications. Hence, calculations are performed here to predict the expected performance of the facility in both regular and non-reflecting shock tunnel modes.

From the experimental data on the speed of the primary shocks shown partly in Fig. 3 of Sec. I, the enthalpies of the flows h for the two shock-tunnel modes are calculated using the recombination rate coefficients given in Ref. 7 as functions of the initial driven-tube charging pressure P_1. The data corresponds to a fixed capacitor voltage of 20 kV and an energy of

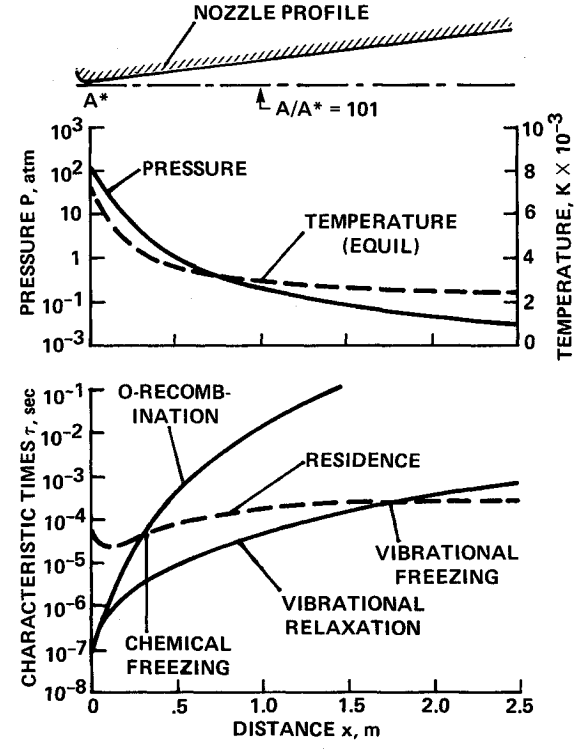

Fig. 7 Calculated typical variation in pressure, temperature, and characteristic residence time for recombination of atomic oxygen, and vibrational relaxation, in a regular shock-tunnel mode at $P_1 = 0.2$ atm, capacitor setting of 20 kV and 172 kJ.

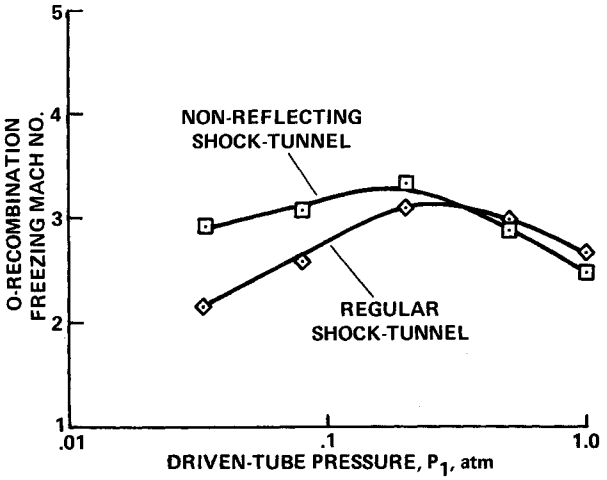

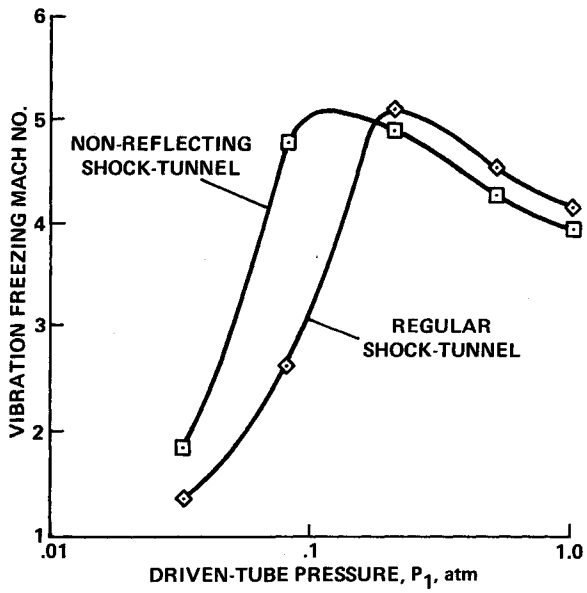

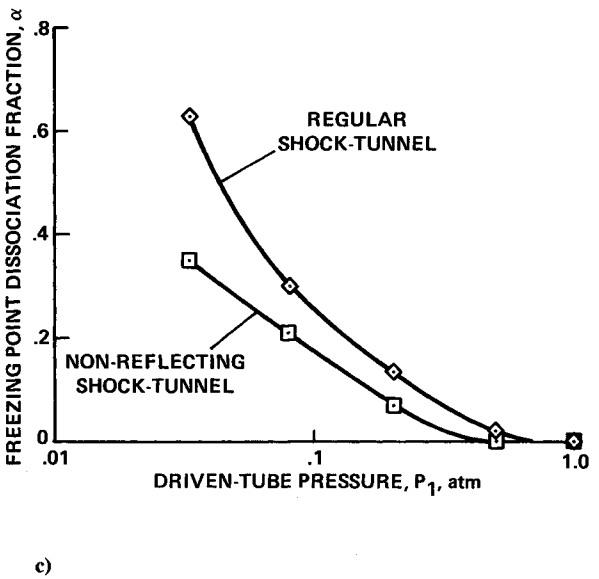

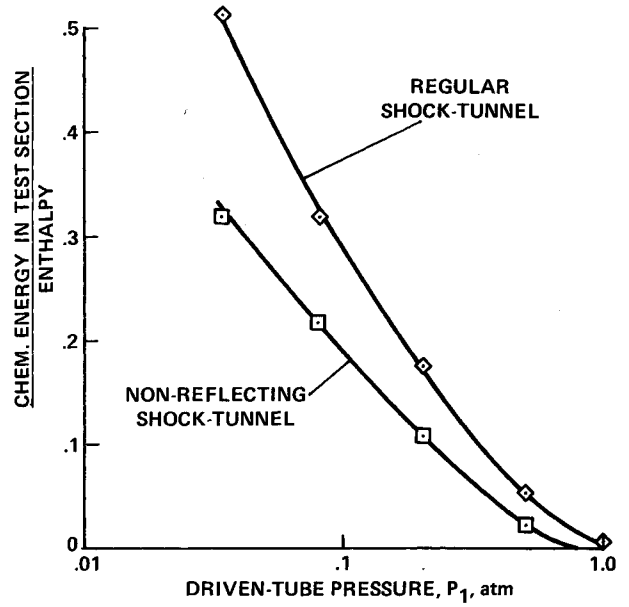

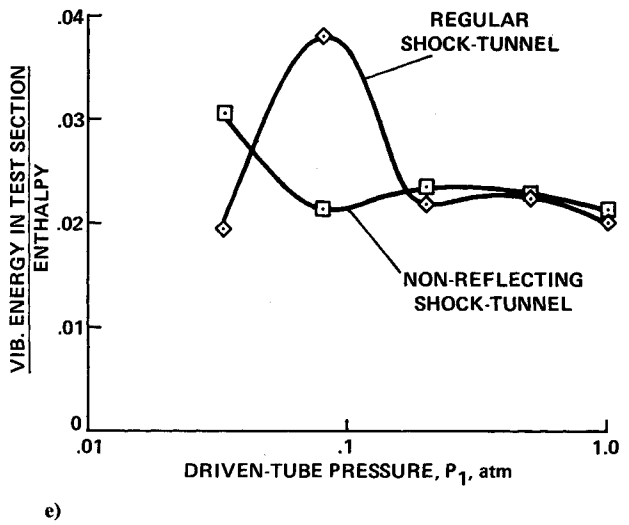

Fig. 8 Calculated freezing-point characteristics in the regular and nonreflecting shock-tunnel modes as functions of the initial driven-tube charging pressure P_1, at a fixed capacitor setting of 20 kV and 172 kJ: a) freezing (frozen) Mach number for the recombination of atomic oxygen; b) freezing (frozen) Mach number of vibrational relaxation; c) dissociation fraction at the freezing point of oxygen recombination; d) ratio of chemical energy to the total enthalpy in the stream after the freezing of oxygen recombination; and e) ratio of vibrational energy to the total enthalpy in the stream after the freezing of vibrational relaxation.

172 kJ over the P_1 range of 0.033–1 atm. The equivalent flight speeds, V_∞ for the regular shock tunnel and V'_∞ for the nonreflecting shock tunnel, are calculated from $h=(1/2)V_\infty^2=(1/2)V'_\infty$. The results are shown in Fig. 5. As seen in the figure, the orbital-entry energy (7.94 km/s) is produced easily in the present facility. The conditions of the produced flows at the starting point of the nozzle, that is, the reflected-shock conditions (condition 5) for the regular shock tunnel and primary-shock conditions (condition 2) for the nonreflecting shock tunnel are plotted in Figs. 6a–6c.

As mentioned in Sec. I, the main difficulty in the shock-tunnel operation is the freezing of the chemical reactions in the nozzle. As the dissociated and vibrationally excited flow ex-

pands through the nozzle, the density and temperature drop so fast that the chemical reactions cannot maintain equilibrium with the local temperature. As a result, the flow in the test section contains atomic species, nitric oxide molecules, which are not found in natural air, and vibrationally excited molecules, even though the local temperature may be cold. If a model is placed in such a stream, the thermodynamic conditions behind the shock waves formed around the model are different from those expected in a flow of quiescent air in chemical equilibrium. As a result, lift, drag, and moments will be different from those in an equilibrium ambient flow.

The chemical and vibrational freezing phenomena have been studied theoretically by many investigators in the past. Understanding of the phenomena is hampered by the lack of knowledge on the energy exchange mechanisms among the internal modes and between the internal modes and the translational mode in such a flow. Experimental data on these phenomena, or the freezing phenomenon in the nozzle itself, are virtually nonexistent.

To assess the possible impact of the freezing phenomena, an attempt is made here to predict the freezing points using the simple Damköhler number criterion. Damköhler number is the ratio of the characteristic flow residence time to the characteristic time required for the chemical reactions. The freezing can be said to occur when the Damköhler number falls below unity. The characteristic chemical reaction time τ_c is calculated from the time needed for the three-body recombination of atomic oxygen:

$$\frac{1}{\tau_c} = \frac{1}{(O)} \frac{d(O)}{dt} = K_r(O)(X)$$

where (O) is the number density of atomic oxygen and (X) is the number density of the mixture. Taking the average of the values given in Ref. 8, K_r is taken to be 10^{15} $(3000/T)$ cm^6 $mole^{-2}s^{-1}$. This criterion assumes implicitly that the oxygen recombination process is the rate-limiting step. The assumption is based on the fact that nitrogen atoms are removed mostly by the exchange reaction

$$N + O_2 \rightarrow NO + O$$

which is much faster than the three-body recombination of oxygen atoms. The NO molecules so formed are removed by the exchange reaction

$$NO + N \rightarrow N_2 + O$$

which is also very fast.

The characteristic vibrational relaxation time is taken to be that of O_2 molecules. It is shorter than that of N_2 molecules but longer than that of NO molecules. The vibrational energies of the three molecular species exchange and equilibrate relatively fast, and so the relaxation time of O_2 and NO molecules will dictate the overall relaxation time even though their concentrations are small. The relaxation time of O_2 molecules is calculated from Ref. 9.

The flow residence time is taken as the time for the flow to travel such a distance that its translational temperature falls by 20%. The nozzle is assumed to be conical to give an area ratio A/A^* of 101 at the distance of 1 m. That is, the area ratio is given by

$$A/A^* = 1 + 100x^2$$

where x is the distance from the throat given in the units of meters. For the calculation of the characteristic times, the flow is assumed to be in equilibrium.

In Fig. 7, typical variation of the three characteristic times is shown for a regular shock-tunnel condition obtained by charging the driven tube at 0.2 atm, at the capacitor setting of 172 kJ. The freezing points of the recombination process and of vibrational relaxation are indicated in the figure.

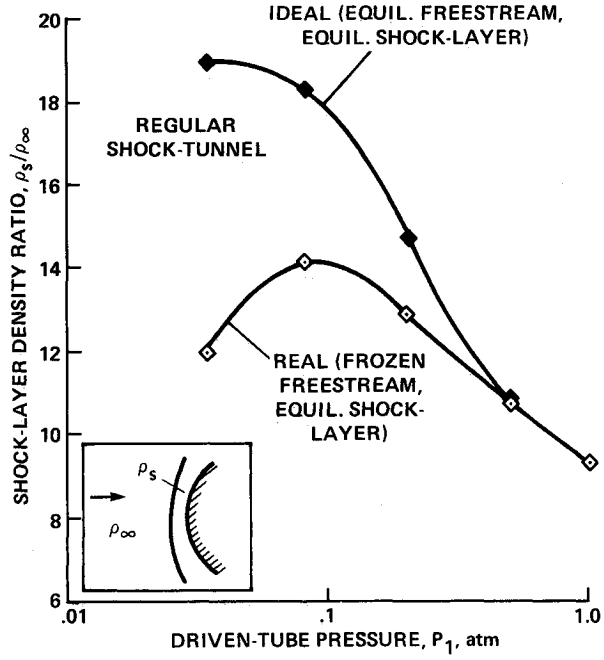

Fig. 9 Comparison between the calculated ideal density ratio between the equilibrium shock layer and the equilibrium freestream and the real density ratio between the equilibrium shock layer and the frozen freestream produced in the present shock tunnel, in a test section where the (equilibrium) temperature is 1000 K, as functions of the initial driven-tube charging pressure, at a fixed capacitor setting of 20 kV and 172 kJ.

In Figs. 8a–8e, the characteristics of the freezing point and the frozen flows are shown as functions of the initial driven-tube charging pressure at the fixed capacitor setting of 172 kJ. As seen in Fig. 8a, the frozen Mach number of the chemical freezing point is between 2 and 3.4 in the present facility. The vibrational freezing Mach number is between 4 and 5.3 if operated at P_1 higher than about 0.1 atm, as seen in Fig. 8b. At lower P_1, vibrational freezing occurs quite early. The dissociation fraction α and the fraction of the energy contained in dissociation are small for P_1 over 0.3 atm, but large for lower P_1, as seen in Figs. 8c and 8d. The energy contained in the vibrational mode after freezing is below 4%. The nonreflecting shock tunnel produces flows closer to equilibrium than the regular shock tunnel.

When a blunt model is placed in the test section and a bow shock wave is formed, and when the model is sufficiently large to produce an equilibrium flow in the shock layer, the density ratio across the normal portion of the bow shock wave ρ_s/ρ_∞ can be calculated for the flows produced in the two shock-tunnel modes in the present facility. The ratio is important because it is a measure of the high-temperature real-gas effect and affects shock shape, which in turn affects pressure distribution over the body. They are shown in Fig. 9 and are compared with the ideal values where the freestream is in chemical equilibrium as in free flight. The density ratio varies from about 9–14 in the present facility as compared to 9–19 in the ideal case. The real ratio obtainable is nearly the same as the ideal value at P_1 values greater than about 0.3 atm. At lower P_1, departure from the ideal values is large.

From Figs. 8d, 8e, and 9, one sees that the present facility simulates the ideal stream fairly closely when the initial driven-tube charging pressure P_1 is over 0.3 atm. Referring to Fig. 5, this means that the facility is capable of reproducing flows to a flight speed below about 5 km/s, or flight Mach numbers of up to about 15. In higher-enthalpy flows produced in the pres-

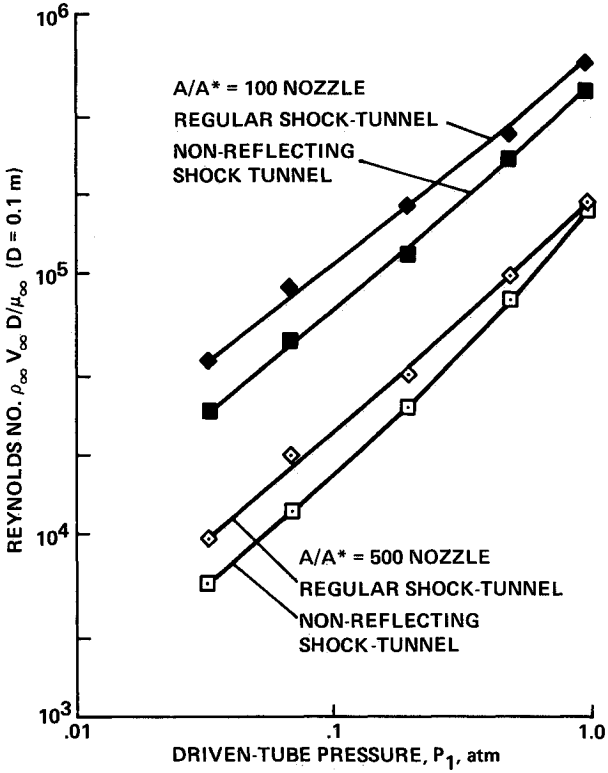

Fig. 10 Calculated Reynolds number based on the density, velocity, and viscosity of the test section stream and a model diameter of 0.1 m, for nozzles of area ratios of 100 and 500, as functions of the initial driven-tube charging pressure P_1, at a fixed capacitor setting of 20 kV and 172 kJ.

ent facility, the freezing phenomena become dominant. As a result, a large fraction of the total enthalpy is contained in the chemical form in the flow at the test section, and the density ratio across a shock wave is appreciably different from that expected in flight. In order to increase the usable enthalpy of the facility, the driven-tube pressures must be increased while maintaining the enthalpy the same. In order to do so, the initial charging pressure of the driver and the electrical energy discharged into the driver must both be increased proportionately. Such upgrading of the arc driver is possible with the use of the predictive methodology described in Sec. I.

In Fig. 10, the Reynolds numbers based on the velocity, density, and viscosity of the flow in the test section and the model diameter of 0.1 m are calculated for the present facility for the nozzles of area ratios of 100 and 500. For P_1 values greater than 0.3 atm, the figure shows that Reynolds numbers in the range of 10^5–6×10^5 are possible with these nozzles.

IV. Conclusions

The stainless-steel driven tube tends to produce metallic impurities when operated at low densities required for the study of nonequilibrium flows. This is avoided by using aluminum for the driven-tube material. The test gas, however, contains carbon contaminants that will have to be removed. The shock-tube facility can produce nonequilibrium flow regimes in air to a shock velocity of up to 13 km/s. The Ames electric-arc shock tubes, when operated as a shock tunnel, can produce enthalpies corresponding to suborbital and to superorbital speeds at pressures sufficient for aerodynamic testing. Calculations show that the flow produced in the test section of a hypersonic nozzle is likely to be almost in equilibrium if the enthalpy is below 12.5 MJ/kg corresponding to a flight speed of 5 km/s. It was found that the chemical freezing occurs at a Mach number of 3 over a wide range of operating conditions.

References

[1]Sharma, S. P., and Park, C., "Operating Characteristics of a 60- and 10-cm Electric Arc-Driven Shock Tube, Part I: The Driver," *Journal of Thermophysics and Heat Transfer,* Vol. 4, No. 3, 1990, pp. 259–265.

[2]Borucki, W. J., "Kerr-Cell-Shuttered $f/1.5$ Stigmatic Spectrograph for Nanosecond Exposures," *Applied Optics*, Vol. 9, No. 2, 1970, pp. 259–264.

[3]Schneider, K. P., and Park, C., "Shock-Tube Study of Ionization Rates of NaCl-Contaminated Argon," *Physics of Fluids*, Vol. 18, No. 8, 1975, pp. 969–981.

[4]Camm, J. C., and Rose, P. H., "Electric Shock Tube for High-Velocity Simulation," AVCO Everett Research Lab., Everett, MA, Research Rept. 136, July 1962.

[5]McKenzi, R. L., "Diatomic Gasdynamic Lasers," *Physics of Fluids,* Vol. 15, No. 12, 1972, pp. 2163–2173.

[6]Shirai, H., and Park, C., "Experimental Studies of Radiative Base Heating of a Jovian Entry Model," *Entry Heating and Thermal Protection: Progress in Astronautics and Aeronautics*, Vol. 69, edited by W. B. Olstad, American Institute of Aeronautics and Astronautics, New York, 1980, pp. 148–171.

[7]Feldman, S., "Hypersonic Gas Dynamic Charts for Equilibrium Air," AVCO Everett Research Labs, Everett, MA, Research Rept. 55, 1957.

[8]Bortner, M. H., "A Review of Rate Constants of Selected Reactions of Interest in Re-Entry in the Atmosphere," U.S. Dept. of Commerce, TN-484, May 1969.

[9]Millikan, R. C., and White, D. R., "Systematics of Vibrational Relaxation," *Journal of Chemical Physics*, Vol. 39, No. 12, 1963, pp. 3209–3213.